Improved 20-32 GHz Atmospheric Absorption Model

Version June 1, 1998

Sandra L. Cruz Pol, Christopher S. Ruf
Communications and Space Science Laboratory, Pennsylvania State University, University Park, PA

Stephen J. Keihm
Jet Propulsion Laboratory, California Institute of Technology, 4800 Oak Grove Drive, Pasadena, CA

Abstract. *An improved model for the absorption of the atmosphere near the 22 GHz water vapor line is presented. The Van-Vleck-Weisskopf line shape is used with a simple parameterized version of the model from Liebe for the water vapor absorption ground truth for comparison with in situ radiosonde derived brightness temperatures under clear sky conditions. Estimation of the new model's four parameters, related to water vapor line strength, line width and continuum absorption, and far-wing oxygen absorption, was performed using the Newton-Raphson inversion method. Improvements to the water vapor line strength and line width parameters are found to be statistically significant. The accuracy of the new absorption model is estimated to be 3% between 20 and 24 GHz, degrading to 8% near 32 GHz. In addition, the Hill line shape asymmetry ratio was evaluated on several currently used models to show the agreement of the data with Van-Vleck-Weisskopf based models, and rule out water vapor absorption models near 22 GHz given by Waters and Ulaby, Moore and Fung which are based on the Gross line shape.*

1. Introduction

Absorption and emission by atmospheric gases can significantly attenuate and delay the propagation of electromagnetic signals through the Earth's atmosphere. Improved modeling of the emission spectra for the dominant contributing gases, mainly water vapor and oxygen, is needed for many applications in communications, remote sensing, and radioastronomy. More precise models of atmospheric absorption can improve corrections for atmospheric effects on satellite observations of land and ocean surfaces [*McMillin,* 1980], produce more accurate remote measurements of atmospheric water vapor burden and temperature profiles [*Grody,* 1980], refine predictions of global climate changes [*NASA*, 1993], enhance planetary radio science measurements [*Pooley,* 1976], improve the accuracy of continental plate motion estimation [*Shapiro et al.,* 1974], and expedite the resolution of accumulated strain at fault zones [*Shapiro,* 1976].

Estimated uncertainties for current models of the 20-32 GHz water vapor absorption range over 4-10% [*Keihm et al*., 1995]. For applications such as water vapor radiometer (WVR) measurements of integrated vapor and cloud liquid used in meteorological and climate modeling, 10% accuracies are often adequate. However, for many applications, especially those requiring calibration of microwave signal delays in the troposphere (path delay), the vapor absorption model uncertainty often dominates experimental error budgets. Examples include the measurement of the vapor-induced path delay over the world's oceans by the TOPEX Microwave Radiometer [*Keihm et al*., 1995] and GEOSAT Follow-on Water Vapor Radiometer [*Ruf et al*., 1996], VLBI geodetic measurements [*Linfield et al*., 1996], and the tropospheric calibration effort planned for the Cassini Gravitational Wave Experiment [*Keihm and March*, 1996].

TABLE 1 New retrieved atmospheric absorption parameters

Parameter	Liebe87-Rosenkranz'93	New Model
C_L	1.0	1.064
C_W	1.0	1.066
C_C	1.2	1.234
C_X	1.0	1.074
RMS difference	1.36 K	1.05 K

Current models for atmospheric microwave absorption have been developed from both laboratory and field experiments. Multimode cavity measurements by *Becker and Autler* [1946] lacked diagnostics necessary to control systematic errors down to a desirable level; their estimated error is between 5% and 10% [*Walter*, 1995]. No comparable laboratory measurements of the 22 GHz feature have been made in the past fifty years. The field measurements of water vapor absorption calibration near the 22 GHz resonance feature generally involve comparisons between direct measurements at two or three selected frequencies by a WVR and theoretical brightness temperatures

calculated from radiosonde (Raob) profiles of temperature, pressure and humidity. Raob comparison measurements [e.g. *Westwater,* 1978; *Hogg et al.,* 1980; *Snider,* 1995] are well known to be subject to inaccurate humidity readings for extreme (very dry or very humid) conditions [*Wade*, 1994; *Nash et al*., 1995].

In this work, radiometric measurements of brightness temperature, T_B, are used in conjunction with *in situ* Raob measurements to estimate parameters for a simplified model of the 20-32 GHz atmospheric vapor and oxygen absorption. The experiment covered ~70 days of near-continuous WVR measurements and twice per day Raob launches at the San Diego and West Palm Beach National Weather Service stations. Advantages over previous such experiments include the use of two independent radiometers for absolute calibration verification, sampling at eight distinct frequencies across the 22 GHz absorption line, and filtering of the Raob data to minimize the effects of high and low end errors in the relative humidity measurements.

A review and comparison of current models are provided in section 2. In section 3, the experiment instrumentation and data processing are described, including steps taken to mitigate known error sources in the Raob data. The analysis, the details of filtering of the data, and the results are presented in section 4, including a recommended new model for the 20-32 GHz spectral region and error estimates. Concluding remarks follow in section 5.

2. Current Models

Currently used models for atmospheric absorption include those by *Liebe and Layton* [1987], *Liebe et al*. [1993], *Waters* [1976] and *Ulaby et al.* [1981]. These will be referred to as L87, L93, W76 and UMF81, respectively, in the remainder of this paper. Figure 1 shows a plot of the water vapor absorption spectrum for each of these models under typical mid-latitude surface conditions. Note that significant differences are evident in both the magnitude and shape of the spectra. Some of the reasons for these differences are discussed below.

Each model includes an empirical continuum term to account for the discrepancy between theoretical and experimental absorption spectra in the window region. The physical phenomena behind the excess absorption in the continuum might be due to inaccuracies in the far wing line shape of vapor resonances [*Gebbie,* 1980], the exclusion of the effects of water clusters [*Bohlander,* 1979] and/or forbidden transitions between energy levels on these line functions [*Rosenkranz*, 1993]. Although this excess has yet to be understood, empirical modifications are needed to obtain more accurate agreement between measurements and theory.

The L87 and L93 models employ the Van Vleck-Weisskopf (VVW) line shape to describe water vapor absorption, whereas the W76 model uses the Gross line shape. The UMF81 uses the Gross line shape for the water vapor and VVW for the oxygen absorption. Both line shapes are derived from a molecular oscillator analogy. In this analogy, the molecule is treated as a classical oscillator with a fixed rotational frequency equal in value to the frequency of the resonant line. Collisions between molecules cause reorientation and rotational phase shifts of the molecule, which contribute to the broadening and shifting of the electromagnetic spectral lines. The basic difference between the two line shape theories is that VVW assumes the oscillations are in phase with the electric field after the collisions, whereas Gross assumes that the molecular oscillation phases stay undisturbed and the post-collision momenta are randomized [*Ben-Reuven*, 1969].

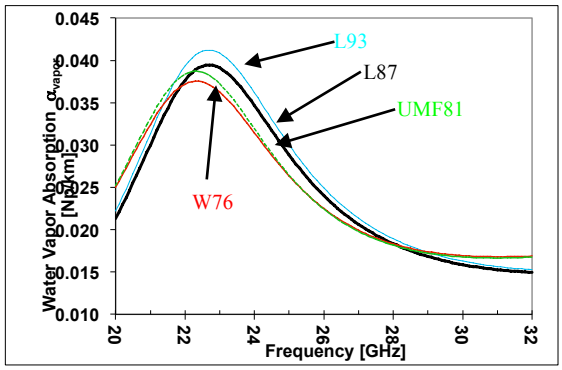

FIGURE 1. Water vapor absorption versus frequency for several models at a pressure of 1013 hPa, air temperature of 290 K and relative humidity of 50%. (L87 = Liebe '87, L93 = Liebe '93, W76 = Waters '76 and UMF81= Ulaby, Moore and Fung '81).

The baseline model which will be refined in this work uses a simplified version of the L87 model for water vapor absorption, in which we have combined the effects of other individual water vapor

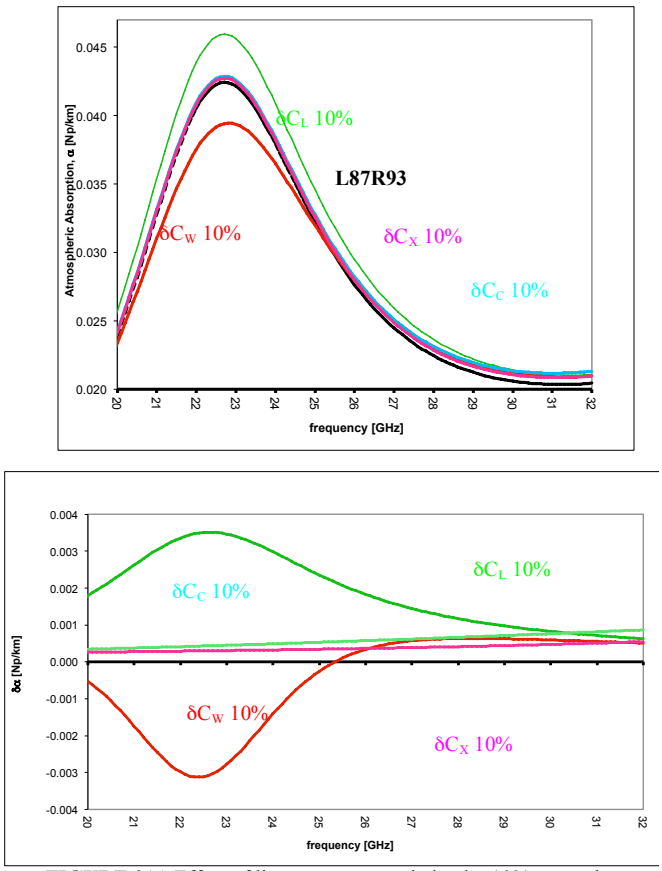

FIGURE 2(a) Effect of line parameter variation by 10% on total atmospheric absorption. **(b)** Differential effect of line parameter variation with respect to nominal L87R93 model. The arrows at the bottom of the figure indicate the frequencies measured in this experiment. (Same atmospheric conditions as Fig.1).

absorption lines, above the 22.235 GHz line, into the continuum term for computational expediency. We have combined the simplified L87 model for water vapor absorption together with the improved oxygen absorption model by *Rosenkranz* [1993]. This model will be referred to as L87R93. Refinements to the water vapor absorption model are accomplished by the addition of three adjustable parameters, C_L, C_W, and C_C, which account for scaling of the line strength, line width, and continuum term, respectively. The oxygen absorption model is refined with the addition of an adjustable scaling factor C_X. Equations for the L87R93 atmospheric absorption model, including all refinement parameters, are included in Appendix A. A selection of C_L =1.0, C_W =1.0, C_C =1.2 and C_X =1.0 yields values within 0.5% of the L87 water vapor absorption model, and the exact *Rosenkranz* [1993] oxygen absorption model, over 20-32 GHz. (Note that the value of the parameter C_C has been raised from 1.0 to 1.2 to account for the wings of the higher water vapor absorption lines.) We refer to these as the nominal values of the C parameters. We note here that the L93 model in the range 20-32 GHz can be reproduced from L87R93 by using the parameters C_L =1.05, C_W =1.0, C_C =1.2 and C_X =1.0. Liebe's increase by 5% in the strength of the water vapor absorption parameter, C_L, from L87 to L93 was in large part due to earlier ground based WVR intercomparisons with Raobs, as reported in *Keihm* [1991]. The line width parameter, C_W, was not adjusted in L93 because the *Keihm* [1991] data set did not include sufficient spectral resolution of the line shape near 22 GHz. Our intent in this work is to reexamine the adjustment that was made to L87 using an improved intercomparison data base. It is for this reason that we begin with L87R93 as our nominal model.

Figure 2a shows the change in absorption spectrum when each of the parameters is increased by 10% above the nominal L87R93 model. The line strength parameter, C_L, increases the absorption significantly, and this increase is accentuated for frequencies near resonance. The width parameter, C_W, increases the width of the curve but at the same time decreases the absorption near the center (resonance) region. Both the continuum, C_C, and the oxygen, C_X, parameters, increase the absorption through the 20-32 GHz frequency span, because of their dependence on the square of frequency. These effects are also depicted in Figure 2b, in which we have plotted the difference in absorption with respect to the nominal L87R93 model.

Uncertainties in attenuation for the L87 water vapor model over tropospheric pressures are estimated to be from 2.3 % to 21.2% [*Liebe and Layton*, 1987]. For the oxygen model used by L87R93 and L93, the uncertainties range from 1.5% to 8% at the nominal frequency of 58 GHz, also for tropospheric pressures [*Liebe et al.*, 1992]. For frequencies away from 58 GHz, the fractional uncertainty can increase significantly.

TABLE 2. Standard deviations and correlation matrix for the four estimated parameters taking into account errors in the Raob profiles and WVR brightness temperature measurements.

Parameter	C_L	C_W	C_C	C_X
Std. Deviation	0.016	.0096	0.155	.252
Parameter	C_L	C_W	C_C	C_X
C_L	1	-0.085	0.045	-0.048
C_W	-0.085	1	-0.513	0.485
C_C	0.045	-0.513	1	-0.989
C_X	-0.048	0.485	-0.989	1

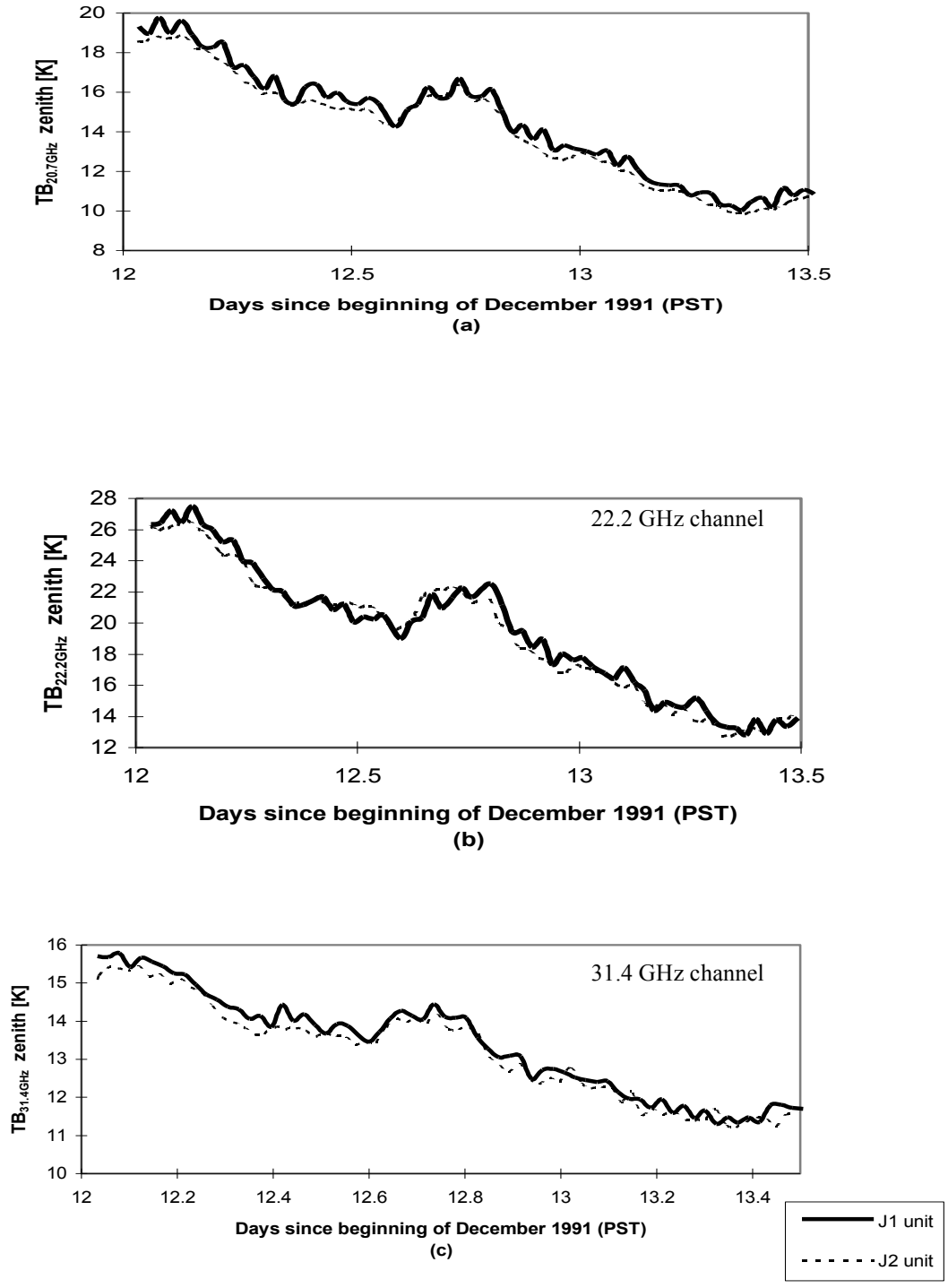

FIGURE 3. Zenith Brightness temperature intercomparison for radiometer units J1 and J2 during December 1991 at San Diego, CA at **(a)** 20.7 GHz, **(b)** 22.2 GHz and **(c)** 31.4 GHz. Measurements have been smoothed by a 30 minutes running average.

3. Experiment Description and Calibration

3.1 Radiometer Data

The experiment consisted of the collection of data at two National Weather Service Radiosonde launch sites. These were chosen for their contrasting humidity conditions to provide constraints on both the 22.235 GHz vapor emission line and the level of oxygen emission in the 20-32 GHz interval. The sites were at San Diego, CA during 11 December 1991 through 3 February 1992 and West Palm Beach, FL during 8 through 21 March 1992. The overall range of humidity in terms of vapor burden varied from 0.6 - 2.9 g/cm^2. Only data obtained under cloud free conditions were used.

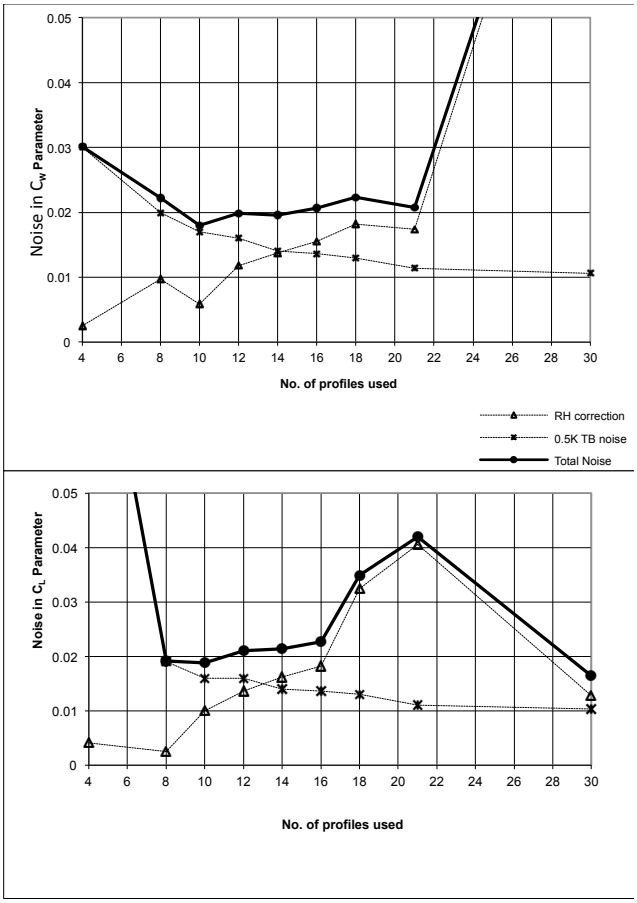

FIGURE 4. Total error in **(a)** C_W and **(b)** C_L line parameters due to a 0.5 K uncertainty in measured T_B and the correction of the Raob relative humidity reading, versus number of Raob profiles used in the estimation (see Section 3.2 for a complete discussion). A trade off between the amount of data used and the minimum error in parameter estimation yields an optimum value of 21 Raob profiles, providing a total of 108 data points at individual frequency channels.

The instruments used included two independently calibrated WVRs, designated J1 and J2, which together provided measurements at 20.0, 20.3, 20.7, 21.5, 22.2, 22.8, 23.5, 24.0 and 31.4 GHz. The J1 Sweeper operated in a continuous tip curve mode at preselected elevation angles from 10^o to 165^o (where 90^o corresponds to the zenith direction) and at up to nine frequencies; 20.0, 20.3, 20.7, 21.5, 22.2, 22.8, 23.5, 24.0 and 31.4 GHz. The J2 WVR included 5 elevation angles and 3 frequencies at 20.7, 22.2, and 31.4 GHz. The J2 unit, which was located approximately 10 m from J1, was only used for the purpose of absolute-calibration verification.

A tip gain calibration [*Elgered*, 1993] was performed on both units. The zenith brightness temperatures were obtained by combining the smoothed gains obtained from the tip curves with antenna and reference counts from longer zenith integrations obtained between tip curves. Only tip data for which the tip-curve fit rms residuals were less than 1.0 K were used for calibration. Poorer quality tip results were deemed unreliable, in terms of absolute calibration, for the purposes of this experiment and often indicated cloudy conditions. The processed high quality tip gains were corrected for beam smearing effects using an opacity- and channel-dependent term derived using the J-series beam pattern. Inter-comparison of T_B data at frequencies common to the J1 and J2 instruments revealed calibration agreement to the < 0.5 K level, as demonstrated in Figures 3(a)-(c). Similarity of the J units would normally lead to concern that common mode instrument errors may be producing absolute calibration errors in excess of the 0.5 K relative agreement. However, in numerous J-unit comparisons with WVRs significantly different in design (*e.g. Keihm* [1991]), relative agreement at the < 0.5 K level was consistently achieved, leading to the conclusion that individual unit absolute calibration < 0.5 K typified WVR performance when operated in the continuous tip curve mode. Only radiometer data from the J1 unit were actually used for comparison with Raob-derived T_B's in the absorption model analysis.

The J1 radiometer T_B data were averaged over one half hour for the times coinciding with the radiosonde balloon launch. This was used as the ground truth for comparison purposes with the Raob-derived T_B's. The 22.8 GHz data was not used due to an unexplained bias in that channel. The eight well-calibrated channels across the full line width of the 22.235 GHz feature constitute an excellent radiometric data set for constraining the line shape model.

3.2 Radiosonde Data

Radiosonde balloons at both sites were released approximately 15 m from the J1 WVR. Raob data were obtained from the National Climatic Data Center (NCDC). These provide height profiles of pressure, air temperature and dew point temperature. The relative humidity was derived from the temperature, dew point and air pressure information using the Goff-Gratch formulation for saturation water vapor density ρ_{ws} [*Goff*, 1949]. See Appendix B for a complete description of the formulation. Note that Goff-Gratch includes a pressure dependence on saturation vapor density, which has been largely neglected in the past. The difference in T_B when including the pressure dependence was found to be up to 1.4K for the raob profiles considered here. This effect was largest for profiles with dry climate conditions.

Indiscriminant use of Raob data can significantly compromise their value as a ground truth standard. We address this problem in the following manner. An estimate is made of the Raob inaccuracies due to known systematic problems with their humidity sensors. Reasonable corrections are then applied to the data. Absorption model parameter estimations are then made both with and without the corrections. We then select only those Raob soundings for which the estimated parameters are minimally affected by the correction. This selection criteria isolates problematic soundings and makes use only of those data in which we have the most confidence.

Between 1973 and October 1993, the National Weather Service routinely truncated their Raob humidity measurements at 20% *RH*, making the radiosonde hygristor appear to lose its sensitivity below 20% *RH* [*Wade*, 1994]. Any humidity below 20% was recorded as 19%. The relative humidities are still reported with a high bias. (See *Wade* [1994] for more details concerning NWS Raob biases). The data also suffered from the inability of the Raob to properly report dew point temperature for levels of relative humidity higher than 95%. To reduce these effects, a correction factor was applied to relative humidity values outside the 20% - 95% range. The relative humidity was set to 11% whenever it was less than 22% (this usually occurred at low altitudes). The *RH* also occasionally exceeded 100% at very high altitudes (typically greater than 8 km). In these cases, we corrected the readings to 20%, which represented a typical reading above 8 km in other profiles, where the *RH* did not exceed 100%. We note, however, that the correction above 8 km had a negligible effect on the present analysis, due to the very low absolute humidity levels at those altitudes.

The determination of which Raob profiles would be used was based on a desire to minimize the effects of their humidity problems without becoming overly sensitive to other measurement errors. The profiles were first ordered according to the magnitude of the change in T_B at 22.2GHz that resulted when the corrections were applied. The first profile in order had less than 0.1K of change. The last profile changed by 12.5K. The four model parameters were then estimated both with and without the corrections, using a variable number of profiles, beginning with the first. Using the first profile alone resulted in the smallest change in estimated parameters with vs. without the correction. Using the first two profiles produced a slightly larger change, and so on, until using all available profiles produced the largest change. This change was then compared with the statistical error in the estimated parameters due to 0.5K Gaussian noise added to the WVR T_Bs. The error in the parameters due to noise will decrease as more profiles are used, due to averaging, whereas the error due to *RH* problems will increase as more problematic profiles are included. Both effects are plotted in Fig. 4a versus the number of profiles used in the estimation, for the case of the width parameter, C_W. The combined root-sum-squared (RSS) error is also plotted. As seen in the figure, the error due to the *RH* corrections is of comparable magnitude to the error introduced by the noise in the WVR T_B when between 10 and 20 profiles are used. The highest number of profiles that can be used without significantly increasing the RSS error in the estimated parameters is found to be 21 profiles. (Each profile is compared with WVR data in the estimation, with up to 8 frequency channels, for a total of 108 data points). The error plots for parameters C_C and C_X look very similar to Fig. 4a. The error plot for the line strength parameter, C_L is shown in Fig. 4b. In Fig. 4b, the RSS error starts increasing at 16 profiles, but at 21 profiles the error is still only 0.04. Based on these results, we select the first 21 profiles to perform the actual parameter estimation. All subsequent analysis presented here is derived from this subset of profiles.

Hoehne [1980] provides estimates of the functional precision for VIZ radiosonde packages as ±0.7 hPa for barometric pressure and ±0.84K for air temperature. *England et al.*, [1993] suggest a value of ±5% be used for relative humidity. Manufacturer's specifications list ±4% for the carbon hygristor humidity sensors used by the VIZ radiosonde, but independent investigations have shown the errors to be dependent on the particular manufactured lot. Therefore, as *England et al.* [1993] note, until more complete investigation of the uncertainties is undertaken, ±5% is a reasonable estimate for the humidity measurements. In any case, the dominant contribution to the error in brightness temperatures inferred from the Raobs comes from the ±0.84K temperature uncertainty and not from the ±5% humidity [*England et al.*, 1993].

4. Analysis and Results

4.1 Hill's Ratio Test

Any of the absorption models described above could in principle be adjusted to fit our data set. In order to select the appropriate absorption models and line shapes, we adopt an asymmetry ratio test formulated by *Hill* [1986]. This test provides a clear-cut means for assessing the validity of the VVW and Gross line shape models and is largely independent of line strength and insensitive to errors in line width, continuum water vapor absorption and oxygen absorption. Two brightness temperatures corresponding to frequencies approximately symmetric about the line center are used to compute the ratio. In this work, 20.7 and 24.0 GHz are used. The ratio is defined as the difference of the two T_Bs divided by their averages,

$$R_T = \frac{T_{B(24.0)} - T_{B(20.7GHz)}}{\left(T_{B(24.0)} + T_{B(20.7)}\right)/2} \qquad (1)$$

The Hill ratio was computed from the Raob-based T_B data for all models mentioned above including the new model presented in this work, and for the WVR data itself. Data obtained at both sites is plotted as a time series in Figure 5. Note that the Hill ratio for the W76 and UMF81 models, both of which use the Gross line shape for the water vapor absorption, yields a much lower value than the corresponding ratio from the WVR data. The W76 and UMF81 models have average ratios of 0.005 and 0.007, respectively, whereas the WVR data has an average ratio of 0.045. The new and L87R93 models, both of which use the VVW line shape, yield average ratios of 0.044 and 0.043, respectively. These results strongly suggest that VVW is the preferred choice for vapor absorption line shape at 22 GHz. Note that the same finding was obtained by *Hill* [1986] when the ratio test was applied to the original *Becker and Autler* [1946] laboratory data.

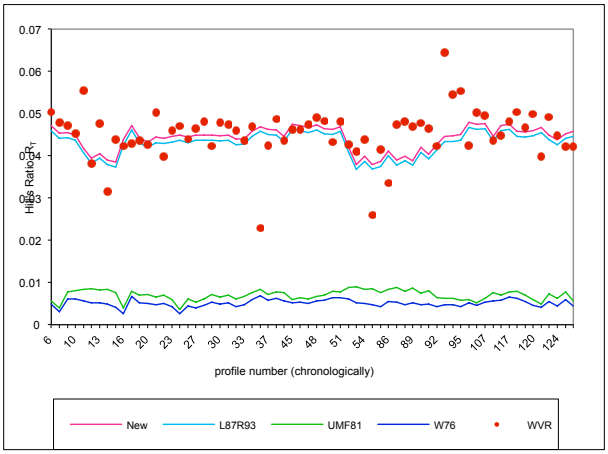

FIGURE 5. Hill ratio comparison between various atmospheric models, showing agreement of the chosen water vapor line shape with the radiometer data, (see text for explanation of models' acronyms).

4.2 Parameter Estimation

The modeled T_B's were calculated using the radiative transfer integral and the parameterized absorption model described in Appendix A applied to the balloon profiles. The parameters C_L, C_W, C_C and C_X were estimated using a Newton-Raphson iterative method [*Kagiwada and Kalaba*, 1969]. The Newton-Raphson method is a fast-converging iterative procedure for non-linear models. The first derivative of the non-linear equation is taken with respect to each of the variables that will be estimated, in this case C_L, C_W, C_C and C_X, which form a vector. The derivative is then evaluated using the initial values for the four parameters to form the Jacobian matrix given by

$$J = \begin{bmatrix} \frac{\partial T_{B1}}{\partial C_L} & \frac{\partial T_{B1}}{\partial C_W} & \frac{\partial T_{B1}}{\partial C_C} & \frac{\partial T_{B1}}{\partial C_X} \\ \frac{\partial T_{B2}}{\partial C_L} & \frac{\partial T_{B2}}{\partial C_W} & \frac{\partial T_{B2}}{\partial C_C} & \frac{\partial T_{B2}}{\partial C_X} \\ \frac{\partial T_{B3}}{\partial C_L} & \frac{\partial T_{B3}}{\partial C_W} & \frac{\partial T_{B3}}{\partial C_C} & \frac{\partial T_{B3}}{\partial C_X} \\ \vdots & \ddots & & \vdots \\ \frac{\partial T_{Bn}}{\partial C_L} & \frac{\partial T_{Bn}}{\partial C_W} & \frac{\partial T_{Bn}}{\partial C_C} & \frac{\partial T_{Bn}}{\partial C_X} \end{bmatrix} \qquad (2)$$

The number of rows in the Jacobian is equal to the number of data points (i.e. the number of Raob profiles times the number of frequencies at each). The number of columns is equal to the number of parameters being estimated. In our case, derivatives were calculated numerically due to the complexity of the radiative transfer integral equation used to compute the T_B. The integration interval for the radiative transfer equation was chosen to be every 30 meters of altitude for adequate precision in the resulting T_B. (The actual Raob samples were unevenly spaced, typically at greater than 30 meter spacings, and so our samples are interpolated accordingly.) The initial values for the four parameters were chosen to be the nominal values, i.e. C_L=1.0, C_W=1.0, C_C=1.2 and C_X=1.0. Then the new C parameters are found as;

$$\vec{c}_{new} = \vec{c}_{initial} + \Delta\vec{c} \qquad (3)$$

where $\Delta\vec{c}$ is the correction for the parameters and is computed from the minimum square error inversion by

$$\Delta \vec{c} = \left(J^t J\right)^{-1} J^t \Delta \vec{T}_B \qquad (4)$$

and $\Delta\vec{T}_B$ is the difference between the $\boldsymbol{T_B}$ modeled with the initial value parameters and the true (observed) $\boldsymbol{T_B}$. These new values for the C's are used as initial values for the next iteration. The process is repeated until changes in each of the parameters are less than 0.001. All four parameters were estimated simultaneously. This is possible because of the number of frequency channels employed and the range of humidity conditions (0.6 - 2.9 g/cm^2 vapor burden) covered during the span of our experiments.

The final estimated parameters, C_L, C_W, C_C and C_X, are shown in Table 1. Figures 6a-c show plots of brightness temperature spectra during the experiment for dry, moderate, and more humid conditions. Each graph plots spectra derived from Raob profiles for both the L87R93 and the new model. Also shown are the coincident radiometer measured brightnesses. The plots demonstrate that the new model agrees more closely with the WVR data. A better indication of this agreement can be seen in Figures 7a-c, where we have plotted the difference in brightness temperature, taking the L87R93 model as the reference. In these figures we have also included the L93 model which, as explained above, is similar to L87R93 except that it has a higher water vapor line strength parameter, (C_L =1.05, C_W=1.0, C_C=1.2 and C_X=1.0). The increase in line strength of the L93 model resulted from measurements at only 21 and 31 GHz [*Keihm*, 1991]. The extra frequencies over 20-32 GHz used to derive our new model can constrain both the shape and strength of the absorption model simultaneously. The result is an increase in both the line strength and width parameters. The new model shows the best agreement with the radiometric temperatures.

The RMS difference between modeled and measured T_B is reduced by 23%, from 1.36K to 1.05K, with the new parameters. A numerical sensitivity analysis was conducted to determine the level of uncertainty in the estimated parameters due to measurement noise by the radiometer and Raobs. Independent realizations of the entire estimation process were simulated, in which random perturbations were made to the actual measurements. Possible biases in the absolute calibration of the radiometer were modeled as an additive constant brightness temperature. Independent biases are determined for each frequency channel, but the bias at a particular channel is assumed constant for all radiosonde launches. Realizations of the biases are selected from a zero mean, normally distributed random process with standard deviation of 0.5 K. Additive random noise in the radiometer data was also modeled. This noise is independent for every channel and Raob profile, and is normally distributed with zero mean and 0.1 K standard deviation. To simulate the uncertainties in Raob measurements, the estimates of precision described in Section 3.2 were used for air temperature, pressure and relative humidity. These Raob errors are incorporated into our sensitivity analysis by assuming that both constant biases and random noise exist in the measurements. For each realization, bias values are selected for air temperature, pressure and relative humidity which are assumed constant over the entire experiment. The values are selected from zero mean, normal distributions with standard deviations of 0.707 times the errors suggested by *Hoehne* [1980] and *England et al.* [1993]. Random noise in each individual measurement is also modeled by zero mean, normal distributions with standard deviations of 0.707 times the published errors. (We note here that the effects of the random noise were found to be negligible relative to the bias errors.) Errors due to the Raob relative humidity "pinning" problems (also discussed in Section 3.2) were modeled in the following manner: For intervals of the profile over which the RH was below 20%, a random humidity level was selected from a uniform distribution between 0 and 20%. For intervals over which the RH was above 100%, a random level was selected from a uniform distribution between 0 and 100%. These ranges bracket the possible uncertainty in our humidity corrections.

The four C parameters were repeatedly estimated with independent errors added to the

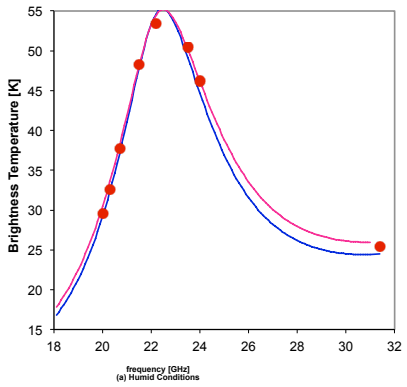

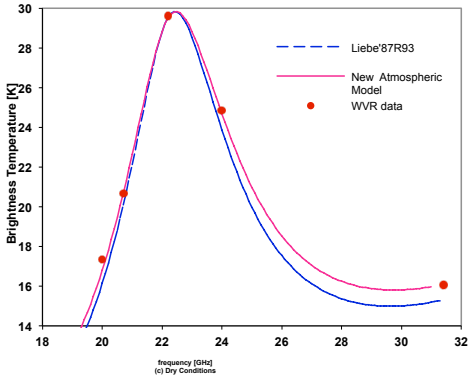

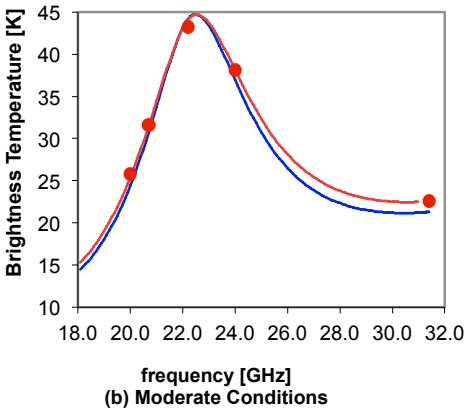

FIGURE 6. Brightness temperature spectra comparison between radiometer data (WVR) and radiosonde-derived data with new and nominal parameters for a vapor burden of **(a)** 2.9 g/cm^2 , **(b)** 2.3 g/cm^2, and **(c)** 1.3 g/cm^2. (Note that only five channels were in operation during the Raob launches for conditions (b) and (c)).

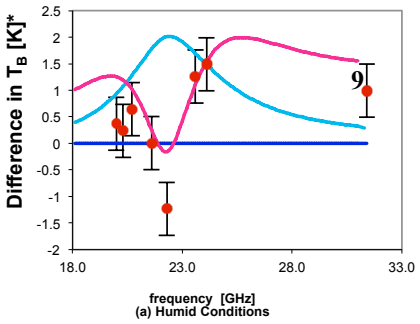

FIGURE 7. Plot of the difference TB -TB_{L87R93} for **(a)** humid (West Palm Beach), **(b)** moderate (San Diego) and **(c)** dry (San Diego) conditions. Note that $TB_{Liebe'87}$ is equivalent to our nominal model (C_L = C_W = C_X =1.0 and C_C = 1.2). (Only five channels were in operation during the Raob launches for conditions (b) and (c)).

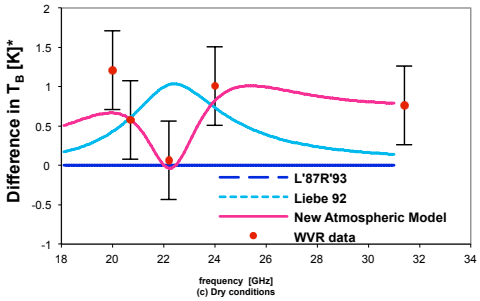

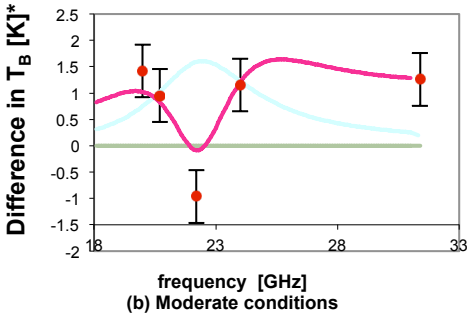

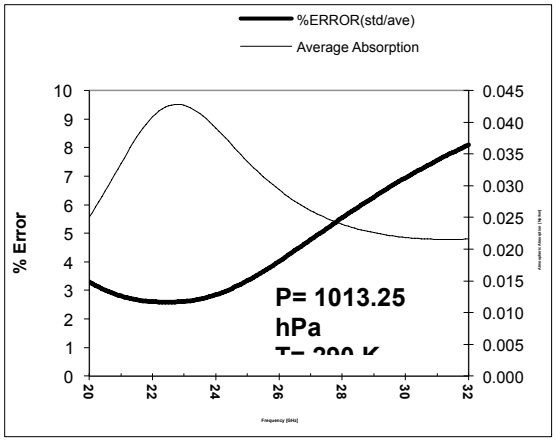

FIGURE 8. Percentage error in the improved model for atmospheric absorption using the 1962 U.S. Standard Atmosphere at sea level with RH = 50%. Model errors are due to bias and random measurement uncertainties in radiometer T_B, the correction for Raob relative humidity values less than 20% or greater than 100%, and the bias uncertainty in the radiosonde readings for pressure, temperature and relative humidity.

data, to obtain 2600 simulated noise realizations. A covariance matrix for the four C parameters was then computed as well as the variance of each of the parameters. The results show that the standard deviations in the C_L and C_W parameters are 1.6% and 0.9%, respectively, and are 16% and 25% for C_X and C_C (see Table 2). Since the standard deviations of the oxygen and continuum parameters, C_X and C_C, are larger than the change from their nominal values, we cannot statistically justify the correction for these two. However, our corrections to the line width and line strength parameters, C_L and C_W, can be considered statistically significant and render a better atmospheric model than the nominal values. Correlation analysis between coefficients shows a high negative correlation of -99% between the errors in the oxygen and continuum terms (C_X and C_C). This is to be expected since both parameters vary essentially as frequency-squared. The correlation among errors in the other parameters vary between ≈ 3% and 52%, as seen in Table 2.

The effect that the errors in the parameters have on the atmospheric model was addressed by a second noise simulation. In this case, 2000 independent realizations were simulated in which the total atmospheric absorption spectrum between 20 and 32 GHz was computed using the surface values of the 1962 U.S. Standard Atmosphere (T=288.15K, P=1013.25 hPa) at a relative humidity of 50%. For each realization, the four C parameters were randomly perturbed according to the standard deviations given in Table 2. From these realizations, mean and standard deviation absorption spectra were computed. The ratio of standard deviation to mean gives the percentage error in the absorption model. The mean and percentage error spectra are shown in Figure 8. The error in the new model is approximately 3% in the near vicinity of the 22 GHz water vapor line, and rises to ≈ 8% near 32 GHz.

5. Conclusions

An improved model for the absorption of the clear atmosphere near the 22 GHz water vapor line is presented. The Van-Vleck-Weisskopf line shape is used with a simplified version of the model by *Liebe* [1987] for the water vapor absorption spectra and the model by *Rosenkranz* [1993] for the oxygen absorption. Radiometric brightness temperature measurements from two sites of contrasting climatological properties, San Diego, CA and West Palm Beach, FL, were used as ground truth for comparison with *in situ* Raob derived brightness temperatures. Estimation of the new model's four parameters, water vapor line strength, line width, and continuum absorption, and far-wing oxygen, was performed using the Newton-Raphson inversion method. In addition, the Hill line asymmetry ratio was evaluated for several currently used models, showing agreement of the radiometric data with the VVW line shape, and ruling out atmospheric absorption models using the Gross line shape near 22 GHz given by *Waters* [1976] and *Ulaby et al.* [1981]. The RMS difference between modeled and measured T_B was reduced from 1.36 K to 1.05 K, with the new parameters. An error analysis shows that the standard deviations in C_L and C_W are 1.6% or less and, 16% and 25% for C_X and C_C, respectively. These errors assume 0.5K bias and 0.1K random errors in the radiometer T_B data, 0.7 hPa bias and random error for pressure, 0.84K for air temperature, and 5% for humidity, and uniformly distributed noise for RH <20% or > 100%. This indicates that our new values for C_L and C_W represent a statistically significant improvement on previous atmospheric absorption models. Our corrections to C_X and C_C are not statistically significant, given the errors associated with the experimental data. The percentage error in the new absorption model is approximately 3% near the 22 GHz line, and rises to 8% near 32 GHz.

The L93 absorption model [*Liebe et al.,* 1993] included a 5% increase in the water vapor line strength above the L87 model [*Liebe and Layton*, 1987]. This increase was largely a result of earlier WVR intercomparisons with Raobs reported in *Keihm* [1991]. Our results here confirm this increase, by proposing a 6% increase (C_L = 1.06)

with a 1.6% margin of error. While our results validate the line strength correction in *Liebe et al.* [1993], they also improve on the line width parameter (C_W = 1.07 ± 0.01). Improvement in the model for line width is possible because our new WVR data set has a greater number of frequency channels across the 22.2 GHz water vapor line.

APPENDIX A — Atmospheric Absorption Model Near 22 GHz.

The water vapor absorption model used in this work is given by

$$\alpha_{water} = 0.0419 f^2 \left[T_L T_S + T_C \right] \quad \text{(A.1)}$$

where, T_L, T_S, and T_C refer to the line strength, line shape and continuum terms and are given by

$$T_L = 0.0109 C_L P_{H_2O} \theta^{3.5} e^{2.143(1-\theta)} \quad \text{(A.2)}$$

$$T_S = \frac{\gamma}{f_o}\left[\frac{1}{(f_o - f)^2 + \gamma^2} + \frac{1}{(f_o + f)^2 + \gamma^2}\right], \quad \text{(A.3)}$$

and,

$$T_C = C_C\left(1.13\times10^{-8} P_{H_2O} P_{\text{dry}}\, \theta^3 + 3.57\times10^{-7} P_{H_2O}^2 \theta^{10.5}\right) \quad \text{(A.4)}$$

The first term in equation (A.4) is due to collisions of the water vapor molecule with foreign molecules like oxygen or nitrogen, while the second term relates to the collision among water molecules. The width parameter, γ, is defined as

$$\gamma = 0.002784\, C_W\left(P_{dry}\, \theta^{0.6} + 4.8\, P_{H_2O}\, \theta^{1.1}\right). \quad \text{(A.5)}$$

In the above equations, θ denotes the temperature ratio, 300/T, where T is the air temperature in Kelvin, P_{dry} denotes the dry air partial pressure, and P_{H2O} the water vapor partial pressure, both in hPa, f denotes frequency in GHz, and f_o is the water vapor resonant frequency, i.e. 22.235 GHz. Equations (A.1)-(A.5) introduce the following parameters: water vapor line strength C_L, line width C_W, and continuum C_C. The above equations agree to within 0.5% with the L87 model over the spectral range of 15-40 GHz when C_L=1.0, C_W=1.0, and C_C=1.2.

The new model parameters (C_L, C_W, C_C , C_X) are on Table 1 above.

The oxygen absorption model used in this work is that of *Rosenkranz* [1993] with the addition of one scaling factor, *Cx*, the oxygen strength parameter. The model is given by

$$\alpha_{oxygen} = C_x \frac{n}{\pi} \sum_{|j|\,odd=0}^{33} S_j(T)\left(\frac{f}{f_j}\right)^2 \left[\frac{\gamma_j + Y_j(f - f_j)}{\gamma_j{}^2 + \left(f - f_j\right)^2} + \frac{\gamma_j - Y_j(f - f_j)}{\gamma_j{}^2 + \left(f + f_j\right)^2}\right] \quad \text{(A.6)}$$

which is equation (2.56) from *Rosenkranz* [1993] with γ_j defined by (2A.4) also from *Rosenkranz* [1993]. In equation (A.6), f is frequency in GHz, f_j is the j^{th} oxygen resonant frequency, and T is air temperature in Kelvin.

APPENDIX B — Goff-Gratch Formulation For Water Vapor Density As A Function Of Temperature And Pressure.

The water vapor density, ρ_w, is a function of both temperature and pressure, [*Goff*, 1949] and it is defined as follows.

$$\rho_w = \rho_{air} \frac{R_w}{R_w + 1}. \quad \text{(B.1)}$$

where ρ_{air} is the air volumetric mass in g/m^3 and is given by

$$\rho_{air} = 348.38 \frac{P}{T_v}. \quad \text{(B.2)}$$

where 348.38 is the reciprocal of the gas constant for dry air (i.e., 1/R=1/[287.04×10^{-3}] = 348.38 for ρ_{air} in g/m^3) and T_v is the virtual temperature is Kelvins

$$T_v = T + T(E - 1)\frac{R_w}{R_w + 1} \quad \text{(B.3)}$$

where E is the apparent molecular weight of dry air (28.966 g) divided by the molecular weight of water (18.016 g), i.e. E = 1.607795. The saturation mixing ratio over water, R_w, is unitless [g/g], and given by

$$R_w = 0.62197 \frac{F_w E_w}{\left(P - F_w E_w\right)} \qquad \text{(B.4)}$$

where E_w is the saturation vapor pressure of water as given by the Goff-Gratch formulation

$$E_w = 10^{\left(I_1 + I_2 + I_3 + \log E_{ws}\right)} \qquad \text{(B.5)}$$

with

$$I_1 = -7.90298\left(T_s / T - 1\right) + 5.02808 \log\left(T_s / T\right) \qquad \text{(B.6)}$$

$$I_2 = -1.3816 \times 10^{-7}\left(10^{\left(11.344\left(1 - T/T_s\right)\right) - 1}\right) \qquad \text{(B.7)}$$

and

$$I_3 = 8.1328 \times 10^{-3}\left(10^{\left(-3.49149\left(T_s/T - 1\right)\right)} - 1\right). \qquad \text{(B.8)}$$

In the above equations, P is air pressure in hPa, T is air or dew point temperature in Kelvins (see paragraph below), $E_{ws} = 1013.246$ hPa is the U.S. Standard Atmospheric pressure near sea, $T_s = 373.14\,\mathrm{K}$ is the boiling point of water, and F_w is a linear fit to the correction factor for the departure of the mixture of air and water from the ideal gas law [*Smithsonian Meteorological Tables* , 1966].

$$F_w = 1 + 10^{-4}\left(5.92854 + 3.740346 \times 10^{-2} P + 1.971198 \times 10^{-4}\left(T - 273.14\right)\left(800 - P\right) + 6.045511 \times 10^{-6} P\left(T - 273.14\right)^2\right). \qquad \text{(B.9)}$$

In the above formulation, the air temperature is used for T to find the saturation vapor density, ρ_{ws}, whereas the dew point temperature is used to find the actual vapor density, ρ_w. The relative humidity is found as

$$RH = \frac{\rho_w}{\rho_{ws}} \times 100 \qquad \text{(B.10)}$$

where ρ_w, and ρ_{ws}, are defined above.

References

Becker, G. E., and S. H. Autler, "Water Vapor Absorption of Electromagnetic Radiation in the Centimeter Wave-length Range," Phys. Rev. , Vol. 70, pp. 300-307, 1946.

Ben-Reuven A., "The Meaning of Collision Broadening of Spectral Lines: The Classical-Oscillator Analog," Adv. in Atm. and Molec. Physics, Ed. by D.R. Bates, I. Estermann, Vol. 5, pp. 201-235, 1969.

Bohlander, R. A., "Spectroscopy of Water Vapor," Ph.D. Thesis, Dept. of Physics, Imperial College, London , 1979.

Elgered, G., "Tropospheric Radio-Path Delay from Ground-Based Microwave Radiometry," Atmospheric Remote Sensing by Microwave Radiometry, Janssen ed., pp.240-243, 1993.

England, M. N., F. J. Schimidlin and J. M. Johansson, Atmospheric Moisture Measurements: A Microwave Radiometer- Radiosonde Comparison, IEEE Trans. Geosci. Remote Sensing, Vol.31, No.2, pp389-398, 1993.

Gebbie, H. A., "Observations of Anomalous Absorption in the Atmosphere," Atmospheric Water Vapor, pp. 133-141, A. Deepak et al editors, Academic Press, 1980.

Goff, J. A., "Final Report of the Working Subcommittee of the International Joint Committee on Psychrometric Data," Trans. Amer. Society of Mechanical Engineers, vol. 71, pp. 903-913, 1949.

Grody, N. C., "Satellite-Based Microwave Retrievals of Temperature and Thermal Winds: Effects of Channel Selection and A Priori Mean of Retrieval Accuracy," Remote Sensing of Atmosphere and Oceans, Ed. by A. Deepak, Academic Press, pp. 381-410, 1980.

Hill, R. J., "Water vapor-absorption line shape comparison using the 22-GHz line : The Van Vleck-Weisskopf shape affirmed," Radio Science, Vol. 21, pp. 447-451, May-June 1986.

Hoehne, W. E., "Precision of National Weather Service upper air measurements," NOAA Tech. Memo. NWS T&ED-16, [NITS Pub. PB81-108316], Boulder, CO, 1980.

Hogg D. C., F. O. Guiraud, C. G. Little, R. G. Strauch, M. T. Decker, and E. R. Westwater, "Design of a Ground-Based Remote Sensing System Using Radio Wavelengths to Profile Lower Atmospheric Winds, Temperature, and Humidity," Remote Sensing of Atmospheres and Oceans, Ed. by Adarsh Deepak, pp. 313-364, 1980.

Kagiwada, H. and R. Kalaba, Newton's method for the nonlinear integral equation for the H function of Isotropic scattering, Santa Monica, CA, Rand Corporation, RM-6030-PR, 1969.

Keihm, S. J., "Water Vapor Radiometer Intercomparison Experiment: Platteville, Colorado, March 1-14, 1991, "Jet Propulsion Laboratory, CA, JPL Task Plan 80-3289, July. 1991.

Keihm S. J., M. A. Janssen, and C. S. Ruf, "TOPEX/Poseidon Microwave Radiometer (TMR):III. Wet Troposphere Range Correction Algorithm and Pre-Launch Error Budget," IEEE Trans. Geosci. Remote Sensing, Vol. 33, No. 1,1995.

Keihm, S. J. and March, "Advanced Algorithm and System Development for Cassini Radio Science Tropospheric Calibration," TDA Progress Report 42-127, pp. 1-19, Jet Propulsion Laboratory, Pasadena, CA, November 10, 1996.

Liebe, H. J., and D. H. Layton, "Millimeter-wave properties of the atmosphere: Laboratory studies and propagation modeling," Nat. Telecom. and Inform. Admin., Boulder, CO, NIT Rep. 87-224, 1987.

Liebe, H. J., G. A. Hufford, and M. G. Cotton, "Propagation modeling of moist air and suspended water/ice particles at frequencies below 1000 GHz," AGARD Conference Proc. 542, *Atmospheric Propagation Effects through Natural and Man-Made Obscurants for Visible to MM-Wave Radiation*, Berlin, May 1993.

Linfield, R. P., S. J. Keihm, L. P. Teitelbaum, S. J. Walter, M. J. Mahoney, R. N. Treuhaft, and L.J. Skjerve, "A test of water vapor radiometer-based troposphere calibration using very long baseline interferometry observations on a 21-km baseline," Rad. Sci. 31, pp. 129-146, 1996

McMillin L. M., "The Split Window Retrieval Algorithm for Sea Surface Temperature Derived From Satellite Measurements," Remote Sensing of Atmosphere and Oceans, Ed. by A. Deepak, Academic Press, pp. 437-452, 1980.

NASA, NASA's Mission to Planet Earth; Earth Observing System, PAM-552, 1993.

Nash, J., Elm J. B., and T. J. Oakley, "Relative Humidity Sensor Performance Observed In Recent International Radiosonde Comparison", Ninth Symposium on Meteorological Observations and Instrumentation, pp. 43-44, Charlotte, NC, American Meteorological Society, March 27-31, 1995.

Pooley, G., "Connected-Element Interferometry," Methods of Experimental Physics: Astrophysics," Ed. by M.L. Meeks, Vol. 12C, Chapter 5.2 , pp. 158-173, Academic Press, NY, 1976.

Rosenkranz, P. W., "Absorption of Microwaves by Atmospheric Gases," Atmospheric Remote Sensing by Microwave Radiometry, Chapter 2, Janssen ed., 1993.

Ruf C. S., R. P. Dewan and B Subramanya, "Combined Microwave Radiometer and Altimeter Retrieval of Wet Path Delay for the GEOSAT Follow-On," IEEE Trans. Geosci. Remote Sensing, Vol. 34, No. 4, July 1996.

Shapiro, I. I., D. S. Robertson, C. A. Knight, C. C. Counselman III, A. E. E. Roger, H. F. Hinteregger, S. Lippincott, A. R. Whitney, T. A. Clark, A. E. Niell, and D. J. Spitzmesser, "Transcontinental Baselines and the Rotation of the Earth Measured by Radio Interferometry," Science, Vol. 186, p 920, 1974.

Shapiro, I. I., "Estimation of Astrometric and Geodetic Parameters," Methods of Experimental Physics: Astrophysics," Ed. by M.L. Meeks, Vol. 12C, Chapter 5.6 , pp. 261-276, Academic Press, NY, 1976.

Smithsonian Meteorological Tables. 6th rev. ed., prepared by Robert J. List. Washington, Smithsonian Institution, 1966.

Snider, J. B., "Observed and theorical atmospheric emission at 20, 30, and 90 GHz: Recent results from land- and ocean- based locations," in Microwave Radiometry and Remote Sensing of the Environment, Ed. by D. Solimini, VSP, Zeist, The Netherlands, 1995.

Ulaby, F. T., R. K. Moore and A. K. Fung, Microwave Remote Sensing :Active and Passive, Vol. 1, pp. 270-278, Addison-Wesley, 1981.

Wade, C. G., "An Evaluation Of Problems Affecting The Measurements Of Low Relative Humidity On The United States Radiosonde", Journal of Atmospherical and Oceanic Technology, Vol. 11, No. 3, pp. 687-700, 1994.

Walter, S. J. and T. R. Spilker, Microwave Resonator Measurements of Atmospheric Absorption Coefficients: A Preliminary Design Study, JPL Publication 95-14, Jet Propulsion Laboratory, CA, 1995.

Waters, J. W., "Absorption and Emission by Atmospheric Gases," Methods of Experimental Physics: Astrophysics," Ed. by M.L. Meeks, Vol. 12B, Chapter 2.3 , pp. 142-176, Academic Press, NY, 1976.

Westwater, E. R., "The accuracy of water vapor and cloud liquid determination by dual-frequency ground-based microwave radiometry," Rad. Sci. 13, 677-685, 1978.